

Ultra-Fast Synthesis of Single-Crystalline Three-Dimensional Covalent Organic Frameworks and Their Applications in Polarized Optics

Lan Peng,[#] Jiang Sun,[#] Jing Huang, Chaoyu Song, Qiankun Wang, Liqian Wang, Hugen Yan, Minbiao Ji, Dapeng Wei, Yunqi Liu, and Dacheng Wei*



Cite This: *Chem. Mater.* 2022, 34, 2886–2895



Read Online

ACCESS |



Metrics & More

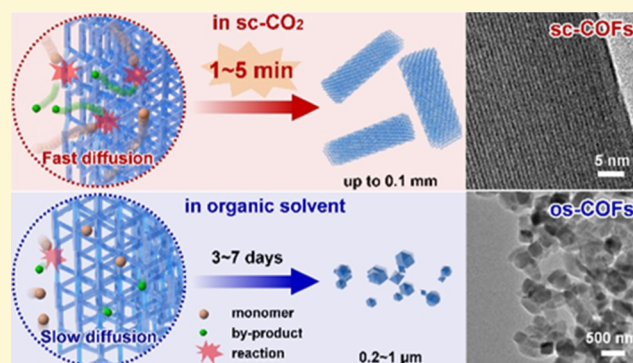


Article Recommendations



Supporting Information

ABSTRACT: The applications of covalent crystalline materials face a chronic challenge of the efficient and precise construction of a highly or single-crystalline product by polymerization, especially for three-dimensional covalent organic frameworks (3D COFs) featuring highly complex crystalline porous structures. Here, we demonstrate the first example of minutes growth of 3D COF single crystals, in which supercritical CO₂ as the solvent extremely accelerates the precise construction of 3D covalent networks. The crystal growth rate of 3D COFs reaches 35 $\mu\text{m min}^{-1}$, and single crystals with sizes up to 110 μm are polymerized within 1–5 min, which have unique optical properties such as polarized photoluminescence, polarized second-harmonic generation, and so on. Considering this, as well as environmental friendliness and industrial compatibility, the supercritically solvothermal polymerization holds great promise in future applications.



INTRODUCTION

Efficient and precise construction of a complex periodic network is of great importance for not only fundamental research but also advanced application of crystalline porous materials.^{1–4} Covalent organic frameworks (COFs), as a type of crystalline porous polymers, are constructed by the atomically precise integration of organic building blocks via stable, usually reversible, covalent bonds in a two-dimensional (2D) or three-dimensional (3D) periodic manner.^{5–7} Owing to the high structural predictability and designability, COFs have been developed for various applications such as photocatalysis, proton conduction, sensing, drug delivery, and so forth.^{8–12} However, the practical utilization of COFs faces a great challenge of the efficient and precise construction of such a complex covalent network, especially 3D COF single crystals.¹³ The growth of single crystals is significant for understanding the structure–function correlation as well as achieving state-of-the-art performance in the applications.

In principle, the formation of strong covalent bonds tends to produce amorphous or poorly crystalline materials.¹⁴ To obtain a crystalline framework, a time-consuming reversible covalent reaction is required for error checking and proof reading,^{15,16} which is restricted by the slow diffusion of reactants and byproducts in a liquid medium. Thus, there is usually a trade-off between the crystallinity of the polymerization product and the reaction time. In other words, higher crystallinity requires longer reaction time. It gives rise to a

fundamental dilemma in the rapid synthesis of highly crystalline frameworks, especially when the whole frameworks, for example, 3D COFs, are assembled by covalent bonds. In addition, 3D COFs, unlike their 2D analogues, lack additional driving forces, such as interlayer π – π stacking, for crystallization and generally feature interlaced and interpenetrated 3D structures, which results in less empty space in the network for building blocks to reach the right place and hinders the mass transfer necessary for the polymerization and crystallization,^{17,18} hence slower reaction rate and poorer crystallinity. Till now, polycrystalline 3D COFs with crystallites from tens to hundreds of nanometers have been prepared by solvothermal or microwave-assisted solvothermal synthesis,^{13,19–24} and the growth normally lasts 1–3 days. To obtain tens of micrometer-sized single crystals of 3D COFs, it is required to add inhibitors that decelerate the crystal growth rate to 0.4–2 nm min^{-1} , and the crystallization is prolonged to 15–80 days.²⁵ The low efficiency, along with disadvantages such as large-scale use of environment-unfriendly organic

Received: July 9, 2021

Revised: March 22, 2022

Published: April 4, 2022



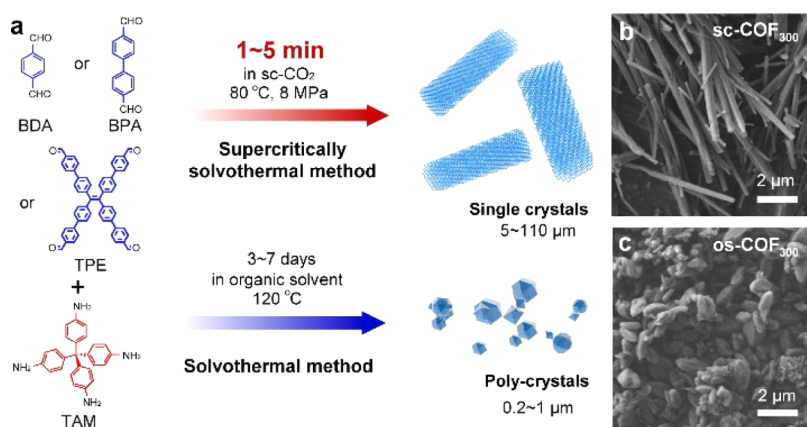


Figure 1. Ultra-fast crystallization of 3D COFs in sc-CO₂. (a) Schematic illustration of supercritically solvothermal synthesis of 3D COFs compared with the solvothermal method. (b,c) FESEM images of the sc-COF₃₀₀ grown for 1 min (b) and the os-COF₃₀₀ grown for 3 days (c), showing distinct morphologies and sizes of 3D COFs synthesized under different conditions.

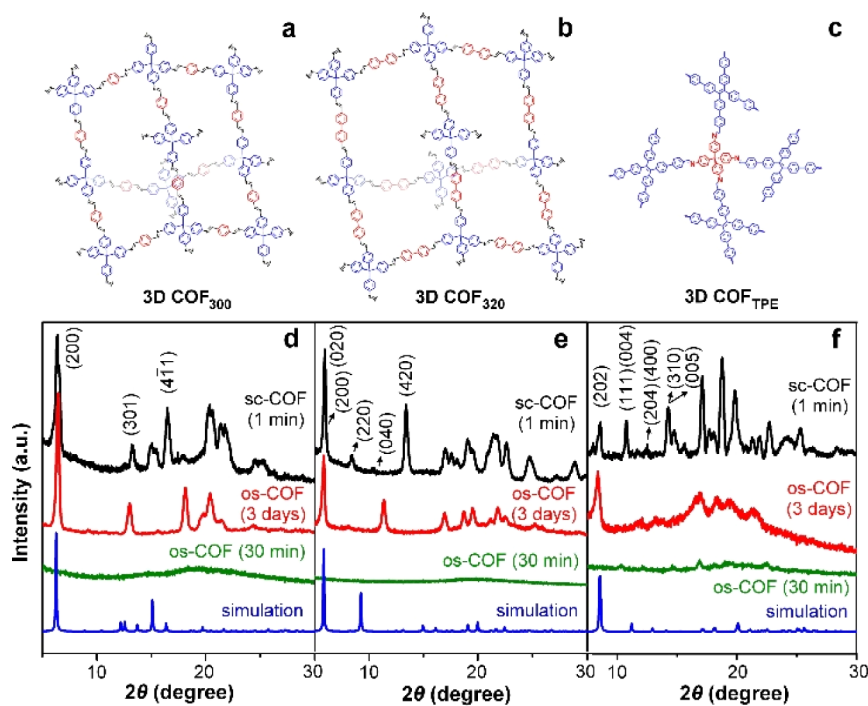


Figure 2. Crystallinity of 3D COFs. (a–c) Chemical structures of COF₃₀₀, COF₃₂₀, and COF_{TPE}. (d–f) PXRD and simulated patterns of COF₃₀₀, COF₃₂₀, and COF_{TPE}, in which sc-COFs are grown for 1 min and os-COFs for 3 days or 30 min, respectively, showing the fast growth of 3D COFs under sc-CO₂ conditions.

solvents, leads to existing synthetic technologies of 3D COFs far away from the requirement of future practical applications.

Supercritical fluid, as a specific medium distinct from gases and liquids, has been widely used in advanced material synthesis and food, coating, and chemical industries.^{26,27} With gas-like diffusivity, viscosity, and surface tension as well as liquid-like density and solvating properties, it greatly enhances the mass transfer and enables a green, scalable, and efficient preparation of nanoparticles, nanowires, films, or foams that cannot be obtained in normal mediums.^{28,29} Here, we find that supercritical CO₂ (termed sc-CO₂) extremely accelerates the reversible reactions for the polymerization of single-crystalline 3D COFs. Based on this finding, we realize supercritically solvothermal synthesis of 3D COF single crystals (termed sc-COFs) with sizes up to 0.11 mm within 1–5 min, around 2–5 orders of magnitude faster than that required for solvothermal

or ionothermal growth of 3D COF single crystals. To the best of our knowledge, it is among the fastest single-crystalline polymerization till now. Although powder X-ray diffraction (PXRD) pattern indicates the coexistence of unreacted monomers and intermediate oligomers with sc-COFs in the product due to the extremely short reaction time, it clearly shows that crystalline 3D COFs have already been synthesized within 1 min, and the single-crystalline nature can be confirmed by transmission electron microscopy (TEM) and selected area electron diffraction (SAED). Besides, we observe polarized photoluminescence (PL) and polarized second-harmonic generation (SHG) from 3D COFs, in agreement with the single crystallinity, showing potential applications of the high-quality 3D COF single crystals in polarized photonics and nonlinear optics.

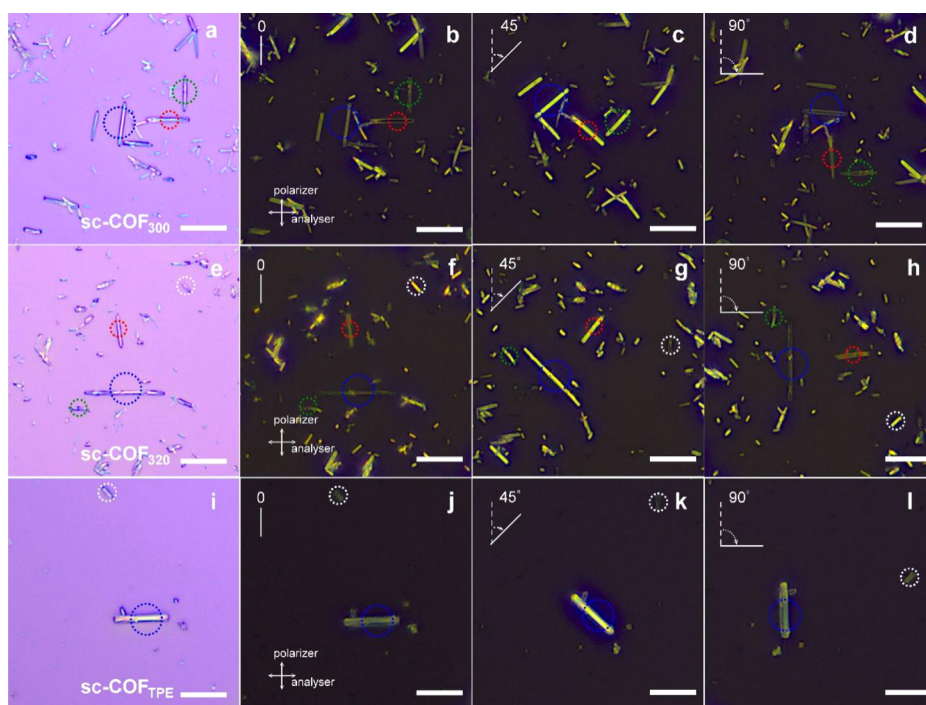


Figure 3. OM images and cross-polarized OM images of sc-COFs. (a) OM image of sc-COF₃₀₀ crystals on a Si/SiO₂ wafer. (b–d) Cross-polarized OM images of sc-COF₃₀₀ when the wafer is rotated by an angle of 0°, 45°, and 90°. (e) OM image of sc-COF₃₂₀ crystals on a Si/SiO₂ wafer. (f–h) Cross-polarized OM images of sc-COF₃₂₀ when the wafer is rotated by an angle of 0°, 45°, and 90°. (i) OM image of sc-COF_{TPE} crystals on a Si/SiO₂ wafer. (j–l) Cross-polarized OM images of sc-COF_{TPE} when the wafer is rotated by an angle of 0°, 45°, and 90°. Uniform polarized light extinction is observed over the entire length of the rods, indicating the single-crystalline nature of the samples. The scale bars are 10 μ m.

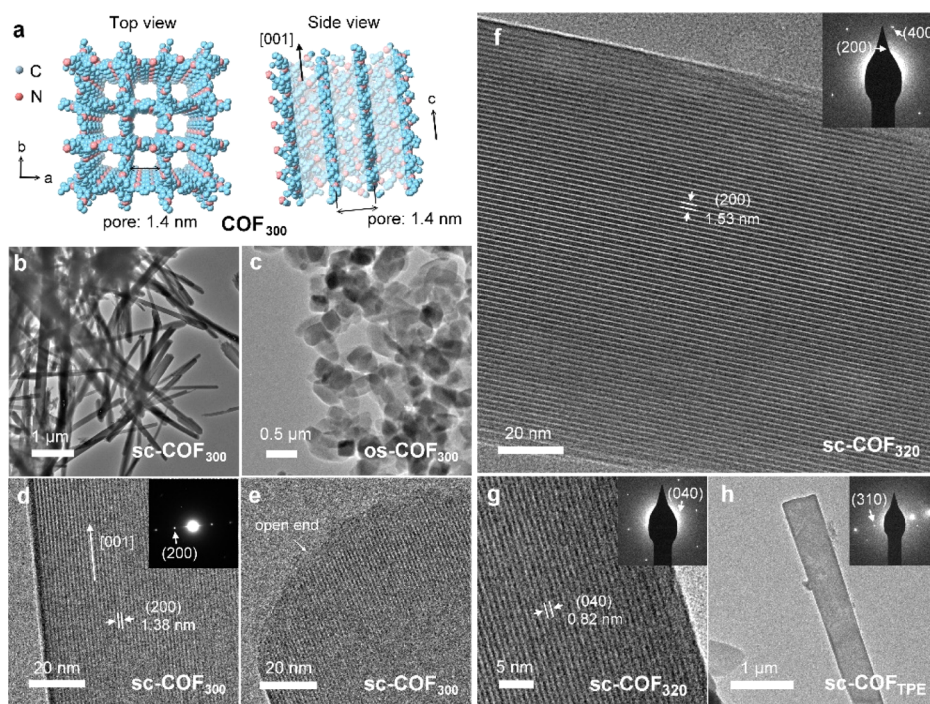


Figure 4. Crystalline structure of 3D COFs. (a) Top and side view of COF₃₀₀. (b,c) TEM images of sc-COF₃₀₀ and os-COF₃₀₀. (d,e) HRTEM images of the middle and the end of sc-COF₃₀₀ single crystals. (f,g) HRTEM images of sc-COF₃₂₀. (h) TEM image of sc-COF_{TPE}. The insets of (d,f–h) are the corresponding SAED patterns. The images verify the single crystallinity of the sc-COF₃₀₀.

RESULTS AND DISCUSSIONS

Supercritically Solvothermal Polymerization. As shown in Figure 1a, three 3D COFs (termed sc-COF₃₀₀, sc-COF₃₂₀, and sc-COF_{TPE}) were synthesized in sc-CO₂ (8 MPa,

80 °C) by using tetrakis(4-aminophenyl)methane (TAM) as the tetrahedral nodes, which reacted with three aldehyde monomers as linkers, namely, benzene-1,4-dicarboxaldehyde (BDA), 4,4'-biphenyldicarboxaldehyde (BPA), and

Table 1. Synthesis Time, Crystal Size, and Growth Rate of 3D COFs

synthesis method	type of 3D COFs	synthesis time	crystal size	growth rate	refs
solvothermal synthesis	imine-based COFs	72 h	JUC-518: 500 nm	0.12 nm min ⁻¹	19
		72 h	JUC-519: 600 nm	0.14 nm min ⁻¹	
	imine-based COFs	72 h	COF-506-Cu: 3 μm	0.7 nm min ⁻¹	20
		5 d	BF-COF-1: 540 nm	0.08 nm min ⁻¹	21
	imine-based COFs	5 d	BF-COF-2: 750 nm	0.1 nm min ⁻¹	
		72 h	COF-320: 1 μm	0.2 nm min ⁻¹	22
	boroxine-linked COFs	4 d	COF-102: <2 μm	0.3 nm min ⁻¹	13
		4 d	COF-103: <2 μm	0.3 nm min ⁻¹	
	boronate ester-linked COFs	9 d	COF-105: <5 μm	0.4 nm min ⁻¹	13
		80 d	LZU-111: 55 μm	0.4 nm min ⁻¹	25
inhibitor-assisted solvothermal synthesis	imine-based COFs	50 d	LZU-79: 100 μm	1.3 nm min ⁻¹	
		15 d	COF-303: 15 μm	0.7 nm min ⁻¹	
		10 d	COF-300: 30 μm	2 nm min ⁻¹	
		25 d	LZU-306: 50 μm	1.3 nm min ⁻¹	42
	boroxine-linked COFs	20 min	COF-102: 30–40 nm	1.5–2 nm min ⁻¹	23
microwave-assisted solvothermal synthesis	anionic COFs	4 h	CD-COF-Li: 0.6–3 μm	2.5–12.5 nm min ⁻¹	24
	imine-based COFs	72 h	COF-300: 1.1 μm	0.25 nm min ⁻¹	43
ventilation vial synthesis	imine-based COFs	3 min	IL-COF-1: 0.6 μm	0.2 μm min ⁻¹	41
ionothermal synthesis	imine-based COFs	12 h	IL-COF-2: 0.2 μm	0.3 nm min ⁻¹	
		12 h	IL-COF-3: 0.7 μm	1 nm min ⁻¹	
		1–5 min	sc-COF ₃₀₀ : up to 85 μm	25 μm min ⁻¹	this work
supercritically solvothermal synthesis		1–5 min	sc-COF ₃₂₀ : up to 66 μm	26 μm min ⁻¹	
		1–5 min	sc-COF _{TPE} : up to 111 μm	35 μm min ⁻¹	

4',4'',4''',4''''-(ethene-1,1,2,2-tetrayl)tetrakis(biphenyl-4-carbaldehyde) (TPE-Ph-CHO), respectively. Sc-CO₂ contained 0.5 vol % *n*-butyl alcohol (*n*-BuOH) as a cosolvent to increase the solubility of monomers. As a comparison, these 3D COFs were solvothermally synthesized in organic solvents, named os-COFs. Optical microscopy (OM) (Figure S1) and field-emission scanning electron microscopy (FESEM) images (Figures 1b,c and S2) show that sc-COFs (grown for 1 min) have rod-like morphologies with a length of several tens of micrometers. The yields of the powder products (grown for 1 min), which are mostly rod-like samples, are 67, 74, and 69% for sc-COF₃₀₀, sc-COF₃₂₀, and sc-COF_{TPE}, respectively. On the contrary, the os-COFs (grown for 3 days) have a yield of 62–75% with rice-shaped or disordered nanoclusters in sub-micrometer dimensions, although the growth time is much longer. If the growth time decreases to 30 min, no or small-yield powder samples are obtained in organic solvents. These results showcase the potential of supercritically solvothermal polymerization in rapid synthesis of high-quality 3D COFs compared with the traditional solvothermal method.

To investigate the chemical structure of the as-prepared samples via the two methods, Fourier transform infrared (FTIR) spectroscopy was carried out, and the spectra of sc-COFs and os-COFs show a C=N typical vibration band at 1620 cm⁻¹, revealing the formation of imine linkages (Figure S3).^{30,31} The ¹³C solid-state nuclear magnetic resonance (¹³C NMR) spectrum of sc-COF₃₀₀ matches that of os-COF₃₀₀ (Figure S4), indicating the same local structure of the materials.^{32,33} PXRD patterns (Figure 2) of sc-COFs (1 min) exhibit characteristic 2θ peaks at low angles of 6.6°, 5.8°, and 8.5°, in agreement with those of os-COFs synthesized for 3 days and the simulation, which correspond to COF₃₀₀ (200), COF₃₂₀ (020), and COF_{TPE} (202), respectively, verifying the fivefold, ninefold, and sevenfold interpenetration topologies of COF₃₀₀, COF₃₂₀, and COF_{TPE}, respectively.^{22,34,35} Although we optimize the experimental conditions, the patterns do not

match well with the simulation patterns in the large angle region (Figure S5). It means that the product still contains some unreacted monomers, intermediate oligomers, or poorly crystallized samples due to the rapid growth rate and extremely short reaction time. Nevertheless, it is clear that some crystalline 3D COFs have been successfully synthesized within 1 min in sc-CO₂. In contrast, os-COFs synthesized for 30 min exhibit no or weak diffraction peaks, which suggests much slower crystallization in organic solvents.

Single-Crystalline Structure. Polarized optical microscopy (POM) images of sc-COFs show polarized light extinction and rebrightening over the crystals after rotation by 45° and 90°, indicating the single-crystalline nature of the samples (Figure 3). To clarify the detailed structure, TEM characterization is performed, and the images (Figures 4 and S6) show a high-yield micrometre-sized rod-like morphology of sc-COFs (1 min), while os-COFs (3 days) are sub-micrometer nanoclusters, in consistency with the FESEM results. In high-resolution TEM (HRTEM) images (Figures 4d–g and S7–S10), continuous nanochannels are clearly observed along the whole rod length of sc-COF₃₀₀ (1 min) and sc-COF₃₂₀ (1 min) and the channels are open at the end (Figure 4e). No grain boundaries or dislocations exist, indicating the high quality and single crystallinity of the samples. The lattice fringe spacing is 1.3 nm and 1.53 nm, corresponding to *d*₂₀₀ for sc-COF₃₀₀ and *d*₂₀₀ for sc-COF₃₂₀, respectively. Owing to 0.5–2 μm thickness of sc-COF_{TPE} (Figure 4g), the electron beam cannot penetrate the samples, precluding to image their lattice structure by HRTEM. SAED is usually used to verify the single crystallinity of various nanomaterials.^{36–40} Here, the sc-COFs are analyzed by SAED, and the SAED patterns are consistent with those in the literature. The diffraction spots vertical to the rod length are indexed to sc-COF₃₀₀ (200), sc-COF₃₂₀ (200), sc-COF₃₂₀ (040), and sc-COF_{TPE} (310) (Figure 4), respectively, indicating highly crystalline structures with the rod length via

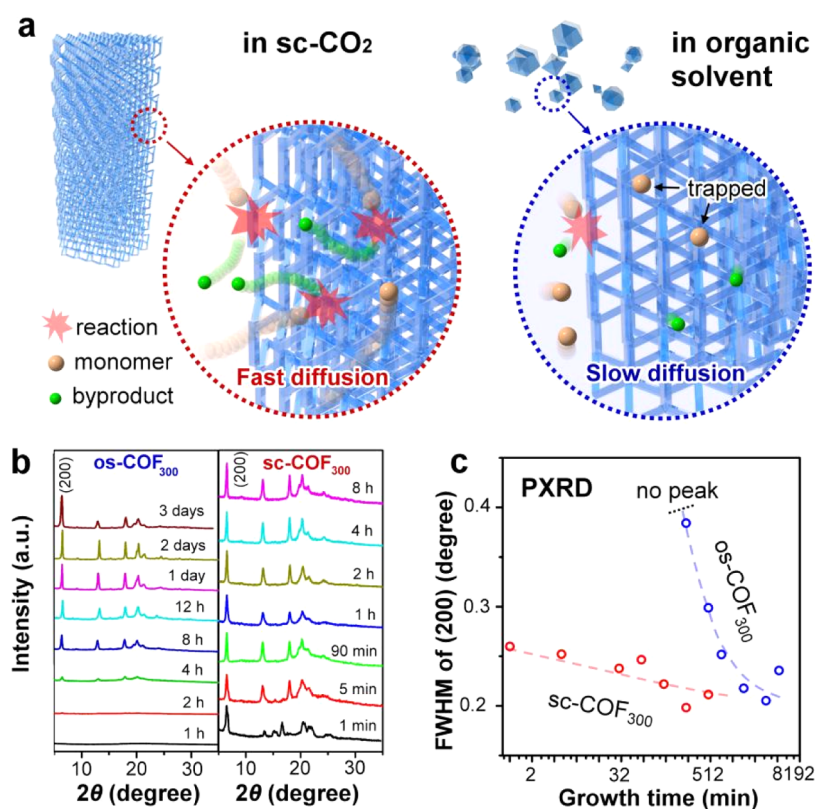


Figure 5. Crystallization mechanism and properties. (a) Schematic illustration of the crystal growth of 3D COFs in sc-CO₂ or organic solvent. (b) PXRD patterns of os-COF₃₀₀ and sc-COF₃₀₀ grown for different times, showing the fast growth of highly crystalline sc-COF₃₀₀ compared to os-COF₃₀₀. (c) FWHM of sc-COF₃₀₀ (200) and os-COF₃₀₀ (200) peaks as a function of the growth time, verifying the high crystallinity of sc-COF₃₀₀ in a short growth time.

[001] direction. When we collect SAED from different locations of one sample, the same set of patterns are obtained (Figure S11), indicating the single-crystalline nature of the sc-COFs.

The growth rate of sc-COFs is up to 35 $\mu\text{m min}^{-1}$, and the crystal lengths grown for 5 min (Figure S12) reach up to 85, 66, and 111 μm for sc-COF₃₀₀, sc-COF₃₂₀, and sc-COF_{TPe}, respectively. To demonstrate the rapid synthesis of large-sized 3D COF single crystals, we summarize the growth rates of different approaches in Table 1. Till now, the best result of growing 3D COF single crystals is only 0.2 $\mu\text{m min}^{-1}$.⁴¹ To address the problem of slow growth, several fast polymerization methods, such as ionothermal or microwave-assisted solvothermal synthesis, have been developed to produce 3D COFs within 3 min to 12 h. However, the domain sizes are only tens to hundreds of nanometers and the growth rates are slower than those obtained in this work,^{23–25} indicating the high potentiality of supercritically solvothermal polymerization in the rapid synthesis of large-sized 3D COF single crystals.

Ultra-Fast Polymerization Mechanism. The ultra-fast crystal growth is closely related to the reaction medium (Figure 5a). In normal cases, the polymerization and crystallization of 3D COFs happen in organic solvents.^{19,24,44,45} Considering the limited reversibility of the covalent bond formation, the error correction for crystallization is time-consuming. The reversibility can be further restricted by the small diffusion coefficient of reactants and byproducts in organic solvents. In addition, 3D COFs have complex interlaced and interpenetrated structures.^{46–48} Owing to the bulkiness and rigidity of the monomers and oligomers,

they are inclined to be kinetically trapped by the 3D frameworks with limited empty spaces, preventing the proximity of reaction groups and further rearrangement into the desired crystalline networks.⁴⁹ These problems result in a fundamental contradiction between the growth rate and the crystalline quality. Thus, large-sized single crystals of 3D COFs can be synthesized only under much slower growth rate by decreasing monomer concentration; however, the crystallization process is prolonged to 15–90 days.²⁵

As a unique reaction medium, supercritical fluid provides a solution to these problems from another perspective, which enormously improves the efficiency and circumvents the kinetic trapping. Specifically, different from organic solvents, sc-CO₂ combines gas-like viscosity and surface tension with liquid-like density and solvating properties.^{50,51} The lower viscosity (about 0.02 cp at 80 °C, 8 MPa, while about 0.3–4 cp of organic solvent) and near-zero surface tension (20–50 dyn cm^{-1}) allow for both much higher penetrating ability and faster diffusion of monomers and oligomers in the medium and the pores of 3D COFs. To prove the capability of sc-CO₂ in promoting the diffusion rate of molecules (Figure S13), we dispersed 5 mg sc-COF₃₀₀ and 5 mg C₆₀ in sc-CO₂ (40 mL), and maintained at 8 MPa, 80 °C for 10 min to 8 h. The samples were washed by dichloromethane three times to remove the surface-adsorbed C₆₀ and were then characterized by Raman spectroscopy. A strong characteristic peak of C₆₀ at 1470 cm^{-1} appears for the 10 min sample (Figure S14), indicating that a large amount of C₆₀ molecules are embedded in micro-pores of sc-COF₃₀₀ even after dichloromethane washing. In the control experiments, we dispersed 5 mg sc-

COF₃₀₀ and 5 mg C₆₀ in anhydrous dioxane (40 mL) and maintained at 120 °C. After washing by dichloromethane, negligible peaks of C₆₀ are observed even when the diffusion time lasts 8 h (Figure S15). This result indicates that sc-CO₂ greatly promotes molecular penetration and diffusion in micropores of 3D COFs compared with the traditional organic medium, facilitating the collision between reactants, hence higher growth rate of 3D COFs.

Besides high penetrating ability and fast diffusion, the local density augmentation of solvent molecules around solute molecules proves to be universal in supercritical fluids, and it is expected to increase the translational diffusion of reactants.^{52,53} These features benefit the fast polymerization along with crystallization because of the following aspects. First, the fast diffusion ensures relatively high concentration of monomers and oligomers as well as relatively low concentration of byproducts near the reaction sites, which increases the polymerization rate compared with that in the organic solvent. Second, the formation and breaking of the covalent bonds are kinetically accelerated, which lead to improved reversibility of the error-checking and proof-reading processes and enable ultra-fast crystallization to form thermodynamically stable single crystals in supercritical fluids. The crystallization route is different from that in the organic solvent. In the organic solvent, the monomers normally tend to form amorphous imine polymers and then transform to crystalline 3D COFs via a long-time reversible reaction. Therefore, owing to the special reaction kinetics in supercritical fluids, 3D COF single crystals can be produced within several minutes.

To clarify the crystallization process, we measured PXRD of sc-COF₃₀₀ and os-COF₃₀₀ after different growth times (Figure 5b). Sc-COF₃₀₀ exhibits high crystallinity within 1 min, and no obvious change in the diffraction peaks occurs even when we extend the reaction time to 8 h, indicating that sc-COF single crystals have already been synthesized even within 1 min. In contrast, it takes 4 h for diffraction peaks of os-COF₃₀₀ to appear, which are rather weak in comparison to 1 min sc-COFs and are significantly enhanced as the synthesis prolongs. Full width at half maximum (FWHM) (Figure 5c), which is related to the crystallinity of the sample, is 0.25° for the (020) peak of sc-COF₃₀₀ (1 min) and slightly decreases to 0.21° after 8 h. By comparison, it decreases from 0.4° (4 h) to 0.22° (3 days) for os-COF₃₀₀, indicating that the products grown in minutes under sc-CO₂ conditions have comparable or higher crystal quality than those grown for hours to days by the solvothermal method.

Applications in Polarized Optics. To explore the potential applications, we studied the PL emission from the sc-COF_{TPE} single crystal. A wide emission peak (Figure S16) appears at 598 nm upon excitation at 488 nm. Angle-dependent PL emission from the single crystal (Figure 6a) is observed when the polarization angle (θ_{PL}) changes from 0° to 180°, where the long-axis direction of the crystal is defined as 0°. The intensity of PL emission becomes stronger when θ_{PL} increases from 0° to 90° and then weaker when θ_{PL} increases from 90° to 180°. The polarized-PL phenomenon is attributed to an anisotropic arrangement of chromophoric groups in the crystal, verifying high crystallinity of sc-COFs.

Second harmonic generation (SHG) is one of the most investigated nonlinear optical processes since the 1960s.⁵⁴ SHG occurs when two incident photons with the same energy at frequency ω interact with the nonlinear medium.⁵⁵ The photons combine to generate a new photon with twice the

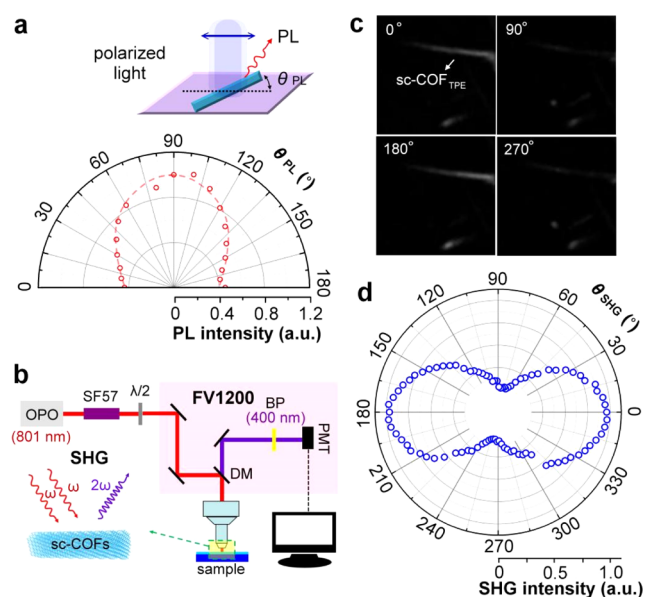


Figure 6. Polarized PL and polarized SHG results of sc-COF_{TPE}. (a) Angle-dependent PL intensity of a sc-COF_{TPE} single crystal at different θ_{PL} from 0° to 180°. (b) Schematic illustration of the nonlinear optical microscopy system for the SHG measurement. (c) SHG images showing the angle-dependent SHG effect of a sc-COF_{TPE} single crystal. (d) SHG polarization polar map of a sc-COF_{TPE} single crystal. The polarized optical properties of the sc-COF_{TPE} single crystal verify its high crystallinity.

energy and a frequency of 2ω . The SHG effect of materials has higher susceptibility than that of other-order nonlinear optical responses by several orders of magnitude, with widespread applications in photonics such as photon generation, bio-imaging, and optical signal transmission and processing.⁵⁶ The SHG signal originates from different types of polarization, which mainly include electric dipole, quadrupole, and so forth, encoding the underlying information of the crystallographic structure with non-centrosymmetry and nonzero nonlinear susceptibility tensors.⁵⁷

SHG images of sc-COF_{TPE} single crystals were acquired by using a nonlinear optical microscopy system with a 150 fs laser centered at 801 nm (Figure 6b). The crystals have strong emission at 400 nm over the whole length of the sample, indicating that the emission originated from intrinsic SHG properties instead of surface effects.⁵⁸ To clarify the crystal symmetry and orientation, we measured the polarization dependence of the SHG signal by rotating the achromatic half-wave plate. The angle-dependent SHG effect of sc-COF_{TPE} is observed (Figure 6c,d). The polarization angle (θ_{SHG}) is defined as the angle between the long-axis direction of the crystal and the polarized direction of the incident laser. The SHG signal gradually decreases when θ_{SHG} increases from 0° to 90° and from 180° to 270°; the SHG signal increases when θ_{SHG} increases from 90° to 180° and from 270° to 360°.

3D COF_{TPE} has no chiral linkers; thus, the SHG effect is not from the chiral topology of dipole orientations.⁵⁸ The SHG signal is related to non-centrosymmetry of the crystal structure. The pts topology of 3D COF_{TPE} is centrosymmetric. Interpenetration is a common phenomenon of 3D COFs that may endow the crystal with non-centrosymmetric space groups.^{13,58} Thus, sc-COF_{TPE} with sevenfold interpenetration topology is non-centrosymmetric, which results in a strong SHG effect from the crystal. Moreover, the polarized SHG

emission shown in Figure 6c,d indicates the high-quality single-crystalline feature of the samples.

CONCLUSIONS

In summary, we realize the supercritically solvothermal synthesis of large-sized 3D COF single crystals as fast as 1 min for the first time. This methodology has advantages such as high efficiency, environmental friendliness without using large amounts of organic solvents, and compatibility with the chemical industry and overcomes existing dilemma in rapid synthesis of highly crystalline or even single-crystalline 3D COFs. Due to the μm^2 -scale sectional area, the rod-like sc-COF single crystals are not suitable for single-crystal X-ray diffraction. Their single-crystalline nature is asserted by TEM and SAED. We observe polarized PL and polarized SHG effects of 3D COFs for the first time, which is characteristic of single crystals, further verifying the single crystallinity of sc-COFs and indicating their special applications in photonics and nonlinear optics. Besides 3D COFs, the supercritically solvothermal method also has great potential in efficient and precise synthesis of other crystalline polymers or porous materials with 3D covalent frameworks. This work provides a new understanding of polymerization in supercritical liquids for rapid crystallization and holds great promise for producing single-crystalline 3D COFs or other materials with state-of-the-art properties in future applications.

EXPERIMENTAL SECTION

Chemicals. BDA (purity $\geq 98\%$) was purchased from Alfa Aesar Chemicals Co. (China). Tetra-(*p*-aminophenyl)-methane (purity $\geq 99\%$), BPA (purity $\geq 98\%$), and 1,1,2,2-tetrakis(4-formyl-(1,1'-biphenyl))ethene (purity $\geq 98\%$) were purchased from Jilin Chinese Academy of Sciences-Yanshen Technology Co. *N*-butyl alcohol (AR, $\geq 99.5\%$), acetic acid (AR, $\geq 99.5\%$), dioxane (AR, $\geq 99.5\%$), mesitylene (AR, $\geq 99.5\%$), and tetrahydrofuran (AR, $\geq 99.5\%$) were purchased from Sinopharm Chemical Reagent Co. Acetone (AR, $\geq 99.5\%$) was purchased from Shanghai Dahe Chemical Co. 1,2-Dichlorobenzene (AR, $\geq 99\%$) was purchased from J&K Scientific Co. Carbon dioxide (purity $\geq 99.99\%$) was purchased from Shanghai Tomoe Gases Co.

Synthesis of 3D COFs. *sc-COF*₃₀₀. A mixture of BDA (5.4 mg, 0.04 mmol) and tetra-(*p*-aminophenyl)-methane (7.6 mg, 0.02 mmol) was dissolved in 200 μL *n*-butyl alcohol (0.5% vol, as a cosolvent) (*n*-BuOH) and 50 μL acetic acid, then transferred to a 40 mL stainless steel reactor. The system was charged with 8 MPa CO₂ with a charging rate of about 1.6 MPa per minute, heated to 80 °C, and reacted for 1 min. After the reaction, the reactor was slowly depressurized at a rate of 1–2 MPa min⁻¹. The precipitate was collected by filtration, washed by acetone and tetrahydrofuran, and dried in a vacuum oven at 100 °C (Scheme S1).

*os-COF*₃₀₀. A mixture of BDA (5.4 mg, 0.04 mmol) and TAM (7.6 mg, 0.02 mmol) was dissolved in 1 mL of anhydrous dioxane and transferred to a reaction tube. After sonication for 5 min at room temperature, the mixture was added to 0.2 mL of 3 M aqueous acetic acid. Then, the tube was degassed through three freeze–pump–thaw cycles, sealed under vacuum, and heated at 120 °C for 3 days. After the reaction, the precipitate was collected by filtration, washed by acetone and tetrahydrofuran, and dried in a vacuum oven at 100 °C.³⁴

*sc-COF*₃₂₀. A mixture of BPA (8.4 mg, 0.04 mmol) and tetra-(*p*-aminophenyl)-methane (7.6 mg, 0.02 mmol) was dissolved in 200 μL *n*-BuOH (0.5% vol, as a cosolvent) and 50 μL acetic acid, then transferred to a 40 mL stainless steel reactor. The system was charged with 8 MPa CO₂ with a charging rate of about 1.6 MPa per min, heated to 80 °C, and reacted for 1 min. After the reaction, the reactor was slowly depressurized at a rate of 1–2 MPa min⁻¹. The precipitate

was collected by filtration, washed by acetone and tetrahydrofuran, and dried in a vacuum oven at 100 °C (Scheme S2).

*os-COF*₃₂₀. A mixture of BPA (8.4 mg, 0.04 mmol) and TAM (7.6 mg, 0.02 mmol) was dissolved in 1 mL of anhydrous dioxane and transferred to a reaction tube. After sonication for 5 min at room temperature, the mixture was added to 0.2 mL of 3 M aqueous acetic acid. Then, the tube was degassed through three freeze–pump–thaw cycles, sealed under vacuum, and heated at 120 °C for 3 days. After the reaction, the precipitate was collected by filtration, washed by acetone and tetrahydrofuran, and dried in a vacuum oven at 100 °C.²²

*sc-COF*_{TPE}. A mixture of 1,1,2,2-tetrakis(4-formyl-(1,1'-biphenyl))-ethene (TPE, 15 mg, 0.02 mmol) and tetra-(*p*-aminophenyl)-methane (TAM, 7.6 mg, 0.02 mmol) was dissolved in 200 μL *n*-BuOH (0.5% vol, as a cosolvent) and 50 μL acetic acid, then transferred to a 40 mL stainless steel reactor. The system was charged with 8 MPa CO₂ with a charging rate of about 1.6 MPa per min, heated to 80 °C, and reacted for 5 min. After the reaction, the reactor was slowly depressurized at a rate of 1–2 MPa min⁻¹. The precipitate was collected by filtration, washed by acetone and tetrahydrofuran, and dried in a vacuum oven at 100 °C (Scheme S3).

*os-COF*_{TPE}. A mixture of TPE (15 mg, 0.02 mmol) and TAM (7.6 mg, 0.02 mmol) was dissolved in 1 mL of anhydrous dioxane and transferred to a reaction tube. After sonication for 5 min at room temperature, the mixture was added to 0.2 mL of 3 M aqueous acetic acid. Then, the tube was degassed through three freeze–pump–thaw cycles, sealed under vacuum, and heated at 120 °C for 3 days. After the reaction, the precipitate was collected by filtration, washed by acetone and tetrahydrofuran, and dried in a vacuum oven at 100 °C.³⁵

Characterization. FESEM images were collected using Zeiss Gemini SEM500; the SEM samples were prepared by dropping COF powder on a clean Si/SiO₂ wafer. OM and cross-polarized OM images were collected using a polarized optical microscope (Leica DM2500P). FTIR spectra were collected using a thermofisher Nicolet 6700 spectrometer. NMR spectra were carried out on a Bruker Advance 400 MHz spectrometer using a standard 4 mm double resonance probe under a spinning speed of 10 kHz. HRTEM images were collected using FEI Tecnai G2 F20 S-Twin (acceleration voltage: 200 kV). PXRD data was collected on a Bruker D8 Advance diffractometer employing Ni filtered Cu K α 1 ($\lambda = 1.54059 \text{ \AA}$) radiation over the range of $2\theta = 5\text{--}35^\circ$ with a step size of 0.02° and 0.15 s per step. Raman spectra were collected by using XploRA (Horiba Jobin Yvon, 785 nm laser).

Angle-Dependent Photoluminescence Measurement.

Angle-dependent photoluminescence (PL) spectra were measured by a Horiba iHR550 spectrometer equipped with a silicon CCD detector array. The excitation source was a 488 nm laser (spot size $\sim 1 \mu\text{m}$, laser power of 70 μW). The incident laser was focused by a Nikon Eclipse Ti microscope with a 50 \times (NA = 0.7) objective. In our experience, the polarization direction of the incident laser light was parallel to the long axis of COF crystals in the measurements. A linear polarizer was placed in the collecting optical path to detect the angle dependence of the PL emission. The polarized PL images were collected using an Olympus BX-51-P fluorescence microscope at different polarization angles (by rotating the stage). A filter set that provided a narrow wavelength range (450–490 nm) was used for excitation and allowed the emitted light at wavelengths above 490 nm to pass to the detector. All optical experiments were performed at room temperature and in ambient environment.

Second Harmonic Measurement. We constructed a nonlinear optical microscopy system to measure the SHG signals of sc-COF_{TPE} samples. The linearly polarized laser beam ($\sim 150 \text{ fs}$, 80 MHz) of 801 nm was generated from a femtosecond optical parametric oscillator (InSight DS+, Newport), chirped into picoseconds ($\sim 3.8 \text{ ps}$) through highly dispersive glass rods (SFS7), sent into a laser-scanning microscope (FV1200, Olympus), and focused onto the samples. The emission photons were collected in an epi mode through the same microscope objective, filtered by a narrow band-pass filter (FF01-405/10-25, Semrock), and detected by a photomultiplier tube (PMT). SHG images were generated by the signals from the PMT. In order to investigate the polarization dependence, a motorized

achromatic half-wave plate (AHP05M-980, Thorlabs) was inserted and rotated before the microscope, and the signal was recorded after every 4°.

■ ASSOCIATED CONTENT

SI Supporting Information

The Supporting Information is available free of charge at <https://pubs.acs.org/doi/10.1021/acs.chemmater.1c02382>.

Additional OM, FESEM, FIR, ¹³C solid-state NMR, TEM, XRD, and PL results (PDF)

■ AUTHOR INFORMATION

Corresponding Author

Dacheng Wei – State Key Laboratory of Molecular Engineering of Polymers, Department of Macromolecular Science, Fudan University, Shanghai 200433, China; Institute of Molecular Materials and Devices, Fudan University, Shanghai 200433, China; Chongqing School, University of Chinese Academy of Sciences, Chongqing 400714, China; orcid.org/0000-0003-3593-9897; Email: weidc@fudan.edu.cn

Authors

Lan Peng – State Key Laboratory of Molecular Engineering of Polymers, Department of Macromolecular Science, Fudan University, Shanghai 200433, China; Institute of Molecular Materials and Devices, Fudan University, Shanghai 200433, China

Jiang Sun – State Key Laboratory of Molecular Engineering of Polymers, Department of Macromolecular Science, Fudan University, Shanghai 200433, China; Institute of Molecular Materials and Devices, Fudan University, Shanghai 200433, China

Jing Huang – Department of Physics, Fudan University, Shanghai 200433, China

Chaoyu Song – Department of Physics, Fudan University, Shanghai 200433, China; orcid.org/0000-0001-9910-9513

Qiankun Wang – State Key Laboratory of Molecular Engineering of Polymers, Department of Macromolecular Science, Fudan University, Shanghai 200433, China; Institute of Molecular Materials and Devices, Fudan University, Shanghai 200433, China

Liqian Wang – State Key Laboratory of Molecular Engineering of Polymers, Department of Macromolecular Science, Fudan University, Shanghai 200433, China; Institute of Molecular Materials and Devices, Fudan University, Shanghai 200433, China

Hugen Yan – Department of Physics, Fudan University, Shanghai 200433, China; orcid.org/0000-0001-8423-6069

Minbiao Ji – Department of Physics, Fudan University, Shanghai 200433, China; orcid.org/0000-0002-9066-4008

Dapeng Wei – Chongqing School, University of Chinese Academy of Sciences, Chongqing 400714, China; orcid.org/0000-0002-3575-617X

Yunqi Liu – Institute of Molecular Materials and Devices, Fudan University, Shanghai 200433, China; Institute of Chemistry, Chinese Academy of Sciences, Beijing 100190, China; orcid.org/0000-0001-5521-2316

Complete contact information is available at:

<https://pubs.acs.org/10.1021/acs.chemmater.1c02382>

Author Contributions

#L.P. and J.S. contributed equally to this work.

Notes

The authors declare no competing financial interest.

■ ACKNOWLEDGMENTS

This work was supported by the National Key Research and Development Program of China (2018YFA0703200), the National Natural Science Foundation of China (61890940), the Strategic Priority Research Program of the Chinese Academy of Sciences (XDB30000000), the Chongqing Talents Program (CQYC2020030146), the Chongqing Bayu Scholar Program (DP2020036), and Fudan University. We would also like to thank the Shiyanjia Lab (www.shiyanjia.com) for the support of materials characterization.

■ REFERENCES

- (1) Zhang, J.-P.; Liao, P.-Q.; Zhou, H.-L.; Lin, R.-B.; Chen, X.-M. Single-Crystal X-Ray Diffraction Studies on Structural Transformations of Porous Coordination Polymers. *Chem. Soc. Rev.* **2014**, *43*, 5789–5814.
- (2) Wang, M.; Luo, D.; Wang, B.; Ruoff, R. S. Synthesis of Large-Area Single-Crystal Graphene. *Trends Chem.* **2021**, *3*, 15–33.
- (3) Fu, H.; Cohen, R. E. Polarization Rotation Mechanism for Ultrahigh Electromechanical Response in Single-Crystal Piezoelectrics. *Nature* **2000**, *403*, 281–283.
- (4) Minemawari, H.; Yamada, T.; Matsui, H.; Tsutsumi, J. Y.; Haas, S.; Chiba, R.; Kumai, R.; Hasegawa, T. Inkjet Printing of Single-Crystal Films. *Nature* **2011**, *475*, 364–367.
- (5) Waller, P. J.; Gándara, F.; Yaghi, O. M. Chemistry of Covalent Organic Frameworks. *Acc. Chem. Res.* **2015**, *48*, 3053–3063.
- (6) Huang, N.; Wang, P.; Jiang, D. Covalent Organic Frameworks: a Materials Platform for Structural and Functional Designs. *Nat. Rev. Mater.* **2016**, *1*, 16068.
- (7) Diercks, C. S.; Yaghi, O. M. The Atom, the Molecule, and the Covalent Organic Framework. *Science* **2017**, *355*, No. eaal1585.
- (8) Vyas, V. S.; Haase, F.; Stegbauer, L.; Savasci, G.; Podjaski, F.; Ochsenfeld, C.; Lotsch, B. V. A Tunable Azine Covalent Organic Framework Platform for Visible Light-Induced Hydrogen Generation. *Nat. Commun.* **2015**, *6*, 8508.
- (9) Bhadra, M.; Kandambeth, S.; Sahoo, M. K.; Addicoat, M.; Balaraman, E.; Banerjee, R. Triazine Functionalized Porous Covalent Organic Framework for Photo-Organocatalytic E-Z Isomerization of Olefins. *J. Am. Chem. Soc.* **2019**, *141*, 6152–6156.
- (10) Xu, H.; Tao, S.; Jiang, D. Proton Conduction in Crystalline and Porous Covalent Organic Frameworks. *Nat. Mater.* **2016**, *15*, 722–726.
- (11) Peng, Y.; Huang, Y.; Zhu, Y.; Chen, B.; Wang, L.; Lai, Z.; Zhang, Z.; Zhao, M.; Tan, C.; Yang, N.; et al. Ultrathin Two-Dimensional Covalent Organic Framework Nanosheets: Preparation and Application in Highly Sensitive and Selective DNA Detection. *J. Am. Chem. Soc.* **2017**, *139*, 8698–8704.
- (12) Bai, L.; Phua, S. Z. F.; Lim, W. Q.; Jana, A.; Luo, Z.; Tham, H. P.; Zhao, L.; Gao, Q.; Zhao, Y. Nanoscale Covalent Organic Frameworks as Smart Carriers for Drug Delivery. *Chem. Commun.* **2016**, *52*, 4128–4131.
- (13) El-Kaderi, H. M.; Hunt, J. R.; Mendoza-Cortés, J. L.; Côté, A. P.; Taylor, R. E.; O’Keeffe, M.; Yaghi, O. M. Designed Synthesis of 3D Covalent Organic Frameworks. *Science* **2007**, *316*, 268.
- (14) Pamplin, B. R. *Crystal Growth: International Series on the Science of the Solid State*; Elsevier Press, 2013.
- (15) Feng, X.; Ding, X.; Jiang, D. Covalent Organic Frameworks. *Chem. Soc. Rev.* **2012**, *41*, 6010–6022.
- (16) Chen, X.; Geng, K.; Liu, R.; Tan, K. T.; Gong, Y.; Li, Z.; Tao, S.; Jiang, Q.; Jiang, D. Covalent Organic Frameworks: Chemical

- Approaches to Designer Structures and Built-in Functions. *Angew. Chem., Int. Ed.* **2020**, *59*, 5050–5091.
- (17) Li, Y.; Chen, W.; Xing, G.; Jiang, D.; Chen, L. New Synthetic Strategies toward Covalent Organic Frameworks. *Chem. Soc. Rev.* **2020**, *49*, 2852–2868.
- (18) Gui, B.; Lin, G.; Ding, H.; Gao, C.; Mal, A.; Wang, C. Three-Dimensional Covalent Organic Frameworks: from Topology Design to Applications. *Acc. Chem. Res.* **2020**, *53*, 2225–2234.
- (19) Li, H.; Chang, J.; Li, S.; Guan, X.; Li, D.; Li, C.; Tang, L.; Xue, M.; Yan, Y.; Valtchev, V.; et al. Three-Dimensional Tetrathiafulvalene-Based Covalent Organic Frameworks for Tunable Electrical Conductivity. *J. Am. Chem. Soc.* **2019**, *141*, 13324–13329.
- (20) Liu, Y.; Ma, Y.; Yang, J.; Diercks, C. S.; Tamura, N.; Jin, F.; Yaghi, O. M. Molecular Weaving of Covalent Organic Frameworks for Adaptive Guest Inclusion. *J. Am. Chem. Soc.* **2018**, *140*, 16015–16019.
- (21) Fang, Q.; Gu, S.; Zheng, J.; Zhuang, Z.; Qiu, S.; Yan, Y. 3D Microporous Base-Functionalized Covalent Organic Frameworks for Size-Selective Catalysis. *Angew. Chem., Int. Ed.* **2014**, *53*, 2878–2882.
- (22) Zhang, Y.-B.; Su, J.; Furukawa, H.; Yun, Y.; Gándara, F.; Duong, A.; Zou, X.; Yaghi, O. M. Single-Crystal Structure of a Covalent Organic Framework. *J. Am. Chem. Soc.* **2013**, *135*, 16336–16339.
- (23) Campbell, N. L.; Clowes, R.; Ritchie, L. K.; Cooper, A. I. Rapid Microwave Synthesis and Purification of Porous Covalent Organic Frameworks. *Chem. Mater.* **2009**, *21*, 204–206.
- (24) Zhang, Y.; Duan, J.; Ma, D.; Li, P.; Li, S.; Li, H.; Zhou, J.; Ma, X.; Feng, X.; Wang, B. Three-Dimensional Anionic Cyclodextrin-Based Covalent Organic Frameworks. *Angew. Chem., Int. Ed.* **2017**, *56*, 16313–16317.
- (25) Ma, T.; Kapustin, E. A.; Yin, S. X.; Liang, L.; Zhou, Z.; Niu, J.; Li, L.-H.; Wang, Y.; Su, J.; Li, J.; et al. Single-Crystal X-Ray Diffraction Structures of Covalent Organic Frameworks. *Science* **2018**, *361*, 48.
- (26) Poliakoff, M.; Licence, P. Green Chemistry. *Nature* **2007**, *450*, 810–812.
- (27) Hobbs, H. R.; Thomas, N. R. Biocatalysis in Supercritical Fluids, in Fluorous Solvents, and under Solvent-Free Conditions. *Chem. Rev.* **2007**, *107*, 2786–2820.
- (28) Loy, D. A.; Russick, E. M.; Yamanaka, S. A.; Baugher, B. M.; Shea, K. J. Direct Formation of Aerogels by Sol-Gel Polymerizations of Alkoxy silanes in Supercritical Carbon Dioxide. *Chem. Mater.* **1997**, *9*, 2264–2268.
- (29) Pai, R. A.; Humayun, R.; Schulberg, M. T.; Sengupta, A.; Sun, J.-N.; Watkins, J. J. Mesoporous Silicates Prepared Using Preorganized Templates in Supercritical Fluids. *Science* **2004**, *303*, 507.
- (30) Ma, J.-X.; Li, J.; Chen, Y.-F.; Ning, R.; Ao, Y.-F.; Liu, J.-M.; Sun, J.; Wang, D.-X.; Wang, Q.-Q. Cage Based Crystalline Covalent Organic Frameworks. *J. Am. Chem. Soc.* **2019**, *141*, 3843–3848.
- (31) Zhao, C.; Diercks, C. S.; Zhu, C.; Hanikel, N.; Pei, X.; Yaghi, O. M. Urea-Linked Covalent Organic Frameworks. *J. Am. Chem. Soc.* **2018**, *140*, 16438–16441.
- (32) Xu, H.-S.; Ding, S.-Y.; An, W.-K.; Wu, H.; Wang, W. Constructing Crystalline Covalent Organic Frameworks from Chiral Building Blocks. *J. Am. Chem. Soc.* **2016**, *138*, 11489–11492.
- (33) Rao, M. R.; Fang, Y.; De Feyter, S.; Perepichka, D. F. Conjugated Covalent Organic Frameworks via Michael Addition-Elimination. *J. Am. Chem. Soc.* **2017**, *139*, 2421–2427.
- (34) Uribe-Romo, F. J.; Hunt, J. R.; Furukawa, H.; Klöck, C.; O’Keeffe, M.; Yaghi, O. M. A Crystalline Imine-Linked 3-D Porous Covalent Organic Framework. *J. Am. Chem. Soc.* **2009**, *131*, 4570–4571.
- (35) Ding, H.; Li, J.; Xie, G.; Lin, G.; Chen, R.; Peng, Z.; Yang, C.; Wang, B.; Sun, J.; Wang, C. An AIEgen-Based 3D Covalent Organic Framework for White Light-Emitting Diodes. *Nat. Commun.* **2018**, *9*, 5234.
- (36) Jash, P.; Nicholls, A. W.; Ruoff, R. S.; Trenary, M. Synthesis and Characterization of Single-Crystal Strontium Hexaboride Nanowires. *Nano Lett.* **2008**, *8*, 3794–3798.
- (37) Mao, Y.; Wong, S. S. General, Room-Temperature Method for the Synthesis of Isolated as Well as Arrays of Single-Crystalline ABO₄-Type Nanorods. *J. Am. Chem. Soc.* **2004**, *126*, 15245–15252.
- (38) Soejima, T.; Kimizuka, N. One-Pot Room-Temperature Synthesis of Single-Crystalline Gold Nanocorolla in Water. *J. Am. Chem. Soc.* **2009**, *131*, 14407–14412.
- (39) Ma, H.; Wan, Z.; Li, J.; Wu, R.; Zhang, Z.; Li, B.; Zhao, B.; Qian, Q.; Liu, Y.; Xia, Q.; et al. Phase-Tunable Synthesis of Ultrathin Layered Tetragonal CoSe and Nonlayered Hexagonal CoSe Nanoplates. *Adv. Mater.* **2019**, *31*, 1900901.
- (40) Robertson, A. W.; Warner, J. H. Hexagonal Single Crystal Domains of Few-Layer Graphene on Copper Foils. *Nano Lett.* **2011**, *11*, 1182–1189.
- (41) Guan, X.; Ma, Y.; Li, H.; Yusran, Y.; Xue, M.; Fang, Q.; Yan, Y.; Valtchev, V.; Qiu, S. Fast, Ambient Temperature and Pressure Ionothermal Synthesis of Three-Dimensional Covalent Organic Frameworks. *J. Am. Chem. Soc.* **2018**, *140*, 4494–4498.
- (42) Liang, L.; Qiu, Y.; Wang, W. D.; Han, J.; Luo, Y.; Yu, W.; Yin, G. L.; Wang, Z. P.; Zhang, L.; Ni, J.; et al. Non-Interpenetrated Single-Crystal Covalent Organic Frameworks. *Angew. Chem., Int. Ed.* **2020**, *59*, 17991–17995.
- (43) Chen, Y.; Shi, Z.-L.; Wei, L.; Zhou, B.; Tan, J.; Zhou, H.-L.; Zhang, Y.-B. Guest-Dependent Dynamics in a 3D Covalent Organic Framework. *J. Am. Chem. Soc.* **2019**, *141*, 3298–3303.
- (44) Lin, G.; Ding, H.; Yuan, D.; Wang, B.; Wang, C. A Pyrene-Based, Fluorescent Three-Dimensional Covalent Organic Framework. *J. Am. Chem. Soc.* **2016**, *138*, 3302–3305.
- (45) Lin, G.; Ding, H.; Chen, R.; Peng, Z.; Wang, B.; Wang, C. 3D Porphyrin-Based Covalent Organic Frameworks. *J. Am. Chem. Soc.* **2017**, *139*, 8705–8709.
- (46) Ma, T.; Li, J.; Niu, J.; Zhang, L.; Etman, A. S.; Lin, C.; Shi, D.; Chen, P.; Li, L.-H.; Du, X.; et al. Observation of Interpenetration Isomerism in Covalent Organic Frameworks. *J. Am. Chem. Soc.* **2018**, *140*, 6763–6766.
- (47) Fang, Q.; Wang, J.; Gu, S.; Kaspar, R. B.; Zhuang, Z.; Zheng, J.; Guo, H.; Qiu, S.; Yan, Y. 3D Porous Crystalline Polyimide Covalent Organic Frameworks for Drug Delivery. *J. Am. Chem. Soc.* **2015**, *137*, 8352–8355.
- (48) Li, Z.; Li, H.; Guan, X.; Tang, J.; Yusran, Y.; Li, Z.; Xue, M.; Fang, Q.; Yan, Y.; Valtchev, V.; et al. Three-Dimensional Ionic Covalent Organic Frameworks for Rapid, Reversible, and Selective Ion Exchange. *J. Am. Chem. Soc.* **2017**, *139*, 17771–17774.
- (49) Ma, X.; Scott, T. F. Approaches and Challenges in the Synthesis of Three-Dimensional Covalent-Organic Frameworks. *Commun. Chem.* **2018**, *1*, 98.
- (50) López-Periágo, A. M.; Domingo, C. Features of Supercritical CO₂ in the Delicate World of the Nanopores. *J. Supercrit. Fluids* **2018**, *134*, 204–213.
- (51) Knez, Ž.; Markočič, E.; Leitgeb, M.; Primožič, M.; Knez Hrnčič, M.; Škerget, M. Industrial Applications of Supercritical Fluids: A Review. *Energy* **2014**, *77*, 235–243.
- (52) Saitow, K.-i.; Otake, K.; Nakayama, H.; Ishii, K.; Nishikawa, K. Local Density Enhancement in Neat Supercritical Fluid due to Attractive Intermolecular Interactions. *Chem. Phys. Lett.* **2003**, *368*, 209–214.
- (53) Mukhopadhyay, M.; Dalvi, S. V. Partial Molar Volume Fraction of Solvent in Binary (CO₂-Solvent) Solution for Solid Solubility Predictions. *J. Supercrit. Fluids* **2004**, *29*, 221–230.
- (54) Zhang, J.; Zhao, W.; Yu, P.; Yang, G.; Liu, Z. Second Harmonic Generation in 2D Layered Materials. *2D Mater.* **2020**, *7*, 042002.
- (55) Streets, A. M.; Li, A.; Chen, T.; Huang, Y. Imaging without Fluorescence: Nonlinear Optical Microscopy for Quantitative Cellular Imaging. *Anal. Chem.* **2014**, *86*, 8506–8513.
- (56) Long, J. P.; Simpkins, B. S.; Rowenhorst, D. J.; Pehrsson, P. E. Far-Field Imaging of Optical Second-Harmonic Generation in Single GaN Nanowires. *Nano Lett.* **2007**, *7*, 831–836.
- (57) Mingabudinova, L. R.; Vinogradov, V. V.; Milichko, V. A.; Hey-Hawkins, E.; Vinogradov, A. V. Metal-Organic Frameworks as

Competitive Materials for Non-Linear Optics. *Chem. Soc. Rev.* **2016**, *45*, 5408–5431.

(58) Chen, Z.; Gallo, G.; Sawant, V. A.; Zhang, T.; Zhu, M.; Liang, L.; Chanthapally, A.; Bolla, G.; Quah, H. S.; Liu, X.; et al. Giant Enhancement of Second Harmonic Generation Accompanied by the Structural Transformation of 7-Fold to 8-Fold Interpenetrated Metal-Organic Frameworks (MOFs). *Angew. Chem., Int. Ed.* **2020**, *59*, 833–838.